SLAC-PUB-12831

INTERACTION REGION ISSUES AT THE NLC

T.W. MARKIEWICZ, T. MARUYAMA
Stanford Linear Accelerator Center, Stanford University, Stanford, CA 94309, USA

Two detector concepts are being investigated for the Next Linear Collider. This paper discusses the current design of the interaction region for one of them, based on a 6 Tesla solenoid and silicon based tracking. Topics include masking layout, backgrounds and the suppression of final quadrupole jitter. All calculations are based on the 1 TeV design parameters.

1 Introduction

Papers which discuss the design issues of the interaction region of an e^+e^- linear collider can be found in the proceedings of this LCWS series of workshops,[1] in the most recent design reports of the NLC, JLC, and TESLA accelerator projects,[2] and in the Proceedings of the 1996 Snowmass workshop on New Directions for High Energy Physics.[3]

In this paper we describe the current interaction region design for the 1 TeV NLC machine. Two detectors, meant to span detector parameter space, are being investigated. This report focuses on the small detector design.

2 IR Layout

Figure 1 shows the current masking and magnet layout in the interaction region (IR) for the NLC Small Detector. In the NLC design, the bunches are separated by 2.8 nsec (although the option of 1.4 nsec separation is being preserved). To avoid parasitic collisions away from the interaction point (IP) the opposing beams must cross at an angle. The design philosophy supposes that it is best to have this angle large enough to extract the beams outside of the nearest magnets to the IP. Currently, each beam enters at ± 10 mrad, for a 20 mrad crossing angle in the horizontal plane, and the nearest quadrupole, $Q1$, begins at $L^*=$ 2m. $Q1SC$ is 30 cm upstream and logically a part of the $Q1$, the vertically focusing member of the final doublet. $Q2$, composed of two physical magnets, occupies the space between 6m and 11m. $Q1$-EXT indicates the start of the quadrupole system that controls the behavior of the disrupted beam after the interaction and transports the beam to its dump. Not indicated in the figure is the RF crab-cavity at $\sim$12m, currently thought to operate in the S-band (2.8 GHz), which will rotate the 100 μm long bunch transversely

Contributed to 4th International Workshop on Linear Colliders (LCWS 99), 04/28/1999--5/5/1999, Sitges, Barcelona, Spain

Work supported by US Department of Energy contract DE-AC02-76SF00515

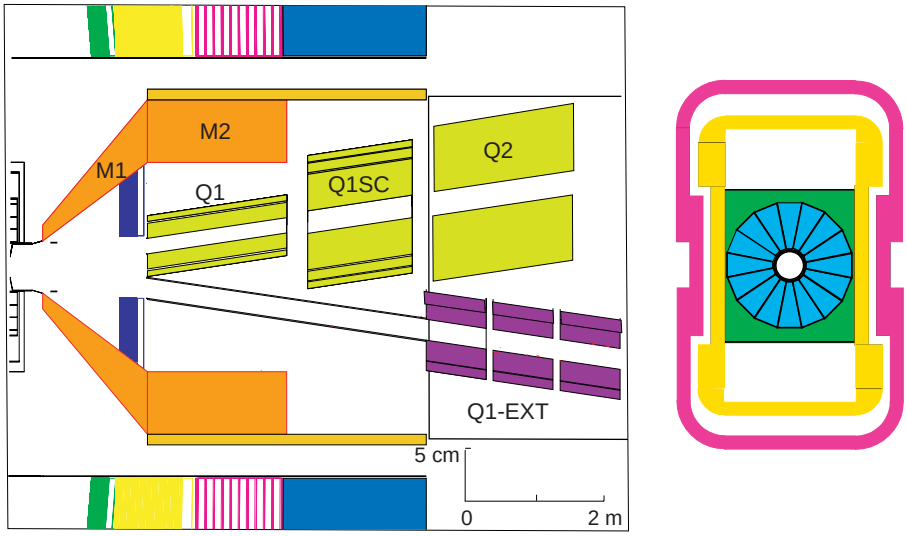

Figure 1: The interaction region masking and magnet layout. At right is the cross section view of the Q1 REC magnet in its stiffening structures. The outer box beam is supported on the cantilevered tube by a mover assembly which corrects for slow position drifts. At high frequencies, the position and orientation of the inner box beam holding $Q1$ is adjusted relative to the outer beam by piezo-electric crystal supports driven by an interferometer or other active device.

so that it collides head-on with the opposing bunch. Low power masks that absorb synchrotron radiation (SR) from the upstream quadrupoles and soft bend magnets, also located in the 11-12 m area, are not indicated.

The design of the IR is necessarily coupled to that of the detector. Figure 1 shows the NLC small detector with its endcaps closed for $r < 40$cm. The strength, shape, and extent of the detector's solenoid field will affect the beam optics, due to the non-zero crossing angles, and the choice of final doublet magnet technology. The overall size and construction will strongly influence the scheme for supporting and stabilizing the final doublet. Background sensitivity is determined by the technology and location of the detector elements. Appropriate masking, such as $M1$ and $M2$ in Figure 1, will help to minimize the observed backgrounds.

2.1 Final Doublet Magnet Technology

In the 1996 ZDR $Q1$ was to be made of wedge shaped blocks of Sm_2Co_{17} rare earth cobalt (REC) permanent magnets. This choice provided a relatively light, and hopefully stiff, magnet, free of cooling fluids, that would work well with an active vibration suppression system. At that time, the extracted beam passed outside the outer radius of $Q1$ into the bore of an essentially identical symmetrically located magnet that was the first optical element of the extraction line. The crossing angle and L^* set the outer magnet radius at 2cm. The bore of the magnet was set by the field gradient required, 33.3 kG/cm for the current lattice, and the desire that the bore not be struck by SR produced in the final doublet itself. The SR calculation depended, in turn, on the amount of beam halo assumed to accompany the beam (1% was assumed) and the level of beam-halo collimation (7 $\sigma_x \times$ 35 σ_y) that the collimation lattice could provide without producing too many muons, without destroying any collimators, and without introducing optical elements with unreasonable tolerances for field quality and vibrational stability. While a bore radius of r =4.5mm was called out, the magnets as described were probably unbuildable.

The detector's field will affect the magnetic properties of the REC material of $Q1$. The axial component of an external field will tend to rotate the REC's magnetic vector out of the plane perpendicular to the $Q1$ axis, thereby reducing the available gradient. The radial component of an external field may cause the REC to demagnetize over time. In the NLC small detector design, the 6 Tesla nominal field is produced by a relatively short 1.55m long coil, leaving the longitudinal and transverse components of the field at z = 2m less than approximately 3 Tesla and 250 Gauss, respectively. Table 1 shows the reduction in pole tip field for Sm_2Co_{17} as a function of external axial field for a typical range of magnetic rigidities found in samples. Early fears that a superconducting flux exclusion tube would be required to protect the REC magnet, thereby negating the advantages that led to its choice as a technology in the first place, have been diminished in light of the actual components of the field map.

Table 1: Reduction of Pole Tip Field of Sm_2Co_{17} in an External Field

External Field	Pole Tip Field Reduction
1.5 Tesla	1.1% - 2.7%
4 Tesla	8% - 21%
6 Tesla	20% - 62%

The current plan is to use the magnetically stiffer Sm_1Co_5 REC for the IP side of $Q1$. The penalty for this is that Sm_1Co_5 has 5% weaker remnants (field strength) than Sm_2Co_{17}. The right side of Figure 1 shows the radial layup of an engineered version of the magnet positioned in a support collar meant to provide longitudinal rigidity. The required pole tip gradient of 19.5 kG/cm is achieved while allowing a bore radius of 6.4 mm. Within this bore is a 0.5mm wall thick stainless beam pipe, of 5.8mm radius aperture, with a clearance to the magnet material of 0.1mm. Longitudinally, the beam pipe is supported independently of the magnet, so that any possible vibration of the vacuum system is not transmitted to $Q1$. The beam pipe aperture is consistent with the SR criteria imposed on the design, as evidenced in Figure 3. Space for realistic engineering tolerances of the magnetic blocks, assembly fixtures, etc. has been allowed for. However, note that all of the available transverse space avalaible at L^* has been used. The first quadrupole in the extraction line has been placed at z =6m, so that only the extraction line beam pipe must be accommodated. Despite the relaxed constraint, the stiffening member around Q1 must be partially removed in the area around L^* to allow for a 1 cm radius (OD) extraction line beam pipe. The next step in the R&D plan for Q1 is to test samples of the material in the near future to determine the maximum allowed external fields.

The $Q1SC$ magnet is meant to provide the tune-ability to accomodate different machine energies. In the small detector layout, $Q1SC$ resides in the return flux of the detector solenoid. Despite the fact that its vibration criteria are on par with that of Q1, on the order of 1 nm, we have continued with the assumption that the magnet will be superconducting. The required field gradient varies from 3.9 kG/cm to 27.8 kG/cm. However, we are uncomfortable with introducing a second demanding technology so close to the REC magnet, and are looking to see how either electromagnets or REC technology could be applied to this magnet.

In the small detector, $Q2$ resides outside the return flux. The only constraint comes from the lateral proximity of the first $Q1$-EXT quad. The current design, which needs engineering input, assumes that the first $Q1$-EXT quads will also be made of REC material in order to minimize the space required. Early designs of conventional iron $Q2$, which deliver the required gradient of 10 kG/cm, indicate that they will barely fit in the space allowed. It may come to pass the the part of $Q2$ closest to the IP is made of REC, while the part further away a tunable conventional iron magnet.

2.2 Beam Optics

The component of the detector's solenoid field perpendicular to the incoming beam would, if uncorrected, have three deleterious effects on the luminosity: 1.) vertical steering would cause the beams to miss each other, 2.) spot size increase due to finite energy spread of the beam (increased dispersion), and 3.) spot size increase due to the emission of SR.

To calculate these effects it is important to use an accurate map of the solenoid field which takes into account the relative position of the coil, return flux, and any other magnetic materials, as well as the coil current density. The NLC small detector design calls for a field of 6 Tesla at the interaction point. Given the current geometry, the longitudinal (transverse) component of the field is less than approximately 3 Tesla (250 Gauss) at $z = 2$m, the IP-end of the innermost final doublet magnet. Without taking some action to ameliorate the effect of the field, using the NLC 1 TeV beam parameters, 1) the beam steering would be 1.7 μm in position and 34 μrad in angle, and the beam spot would increase by 2) 34 μm due to dispersion and 3) some small number of nm due to SR (increasing rapidly with higher energy).

Early solutions to this problem were based on either surrounding the final quadrupoles in a superconducting flux exclusion tube or providing $\approx$800 G-m of dipole steering inboard of the final quad, both highly undesirable. It has been realized [4], however, that appropriate adjustment of the NLC's skew quad correction system can essentially negate the effects of the detector solenoid at the expense of a slightly more complicated machine setup. After this adjustment, the luminosity loss at the IP due to the solenoid effect is less than 1.2% and we must only consider the residual steering effects in position (410 μm) and angle (69 μrad) at the entrance to the extraction line. The current plan is to run only with the detector solenoid on and to realign the extraction line when the beam energy is changed.

3 Vibration Control

The NLC small detector was chosen as a starting point for the IR design because it seems to allow for a simpler support scheme for the final doublet. We assume that there will be an extension of the tunnel into the detector pit that will provide a steady reference platform upon which $Q2$ and the extraction line can be mounted. The door of the detector will open up to this point. The overall support plan (Figure 1) calls for $Q1SC$ and $Q1$ to be supported on precision mover assemblies, similar to those used at FFTB, which are mounted in a 25cm radius 1 inch wall aluminum support tube that is cantilevered from

a support point at the lip of the reference platform.

3.1 Slow control

The support/mover assembly has been designed for $Q1$; for the moment we assume that a similar platform can be designed for $Q1SC$. Five motor-driven cams control the 5 degrees of freedom of the $Q1$ assembly in its stiffening structure (z is fixed). A slow feedback system, similar to that used with great effectiveness by the SLC, and based on beam-beam deflections, will be used to drive the system and stabilize Q1 for variations below about 1 Hz in frequency. The cams will provide the range of adjustment required while the piezo supports described in the following section will provide nm level positioning resolution. For example, a 1°C change in temperature over 12 hours, will produce a 1 nm/sec drift in the size of a 5m steel object, a typical dimension in a detector which might provide the support for a magnet.

3.2 Optical Anchor

It is hoped that the site chosen for the NLC and its IR is seismically quiet, that all precautions have been taken to avoid the coupling of "cultural" vibrations of nearby pumps and compressors to the final doublet, and that the detector and magnet supports have been designed so that any resonances are beyond the frequency range of interest. As these features may not be possible to achieve, since the time of the ZDR, we have assumed that, for frequencies higher than ∼1Hz, we would control vibration motion of the doublet elements by using an appropriate sensor array to drive a system of piezoelectric crystal supports. While we have thought about using either inertial sensors or optical interferometers as the sensing element, at this time only R&D on the interferometer based system has been carried out [5].

We have seen that the fringe pattern of interferometers with either 1m arms or 10m arms can me made stable to better than 1nm by either locating them in quiet settings or by adjusting the path length of one of the arms with a mirror driven by a piezo crystal whose input signal is derived from the fringe pattern. The interferometer arms must by encased in tubes to avoid air motion, but, so far, they need not be either evacuated or gas filled. Using geophones, we have measured the vibrational modes of a 100kg test mass system that is meant to simulate the mechanical properties of a magnet. The next step is to try to incorporate the interferometer system with the test mass to begin to study the problems of a real system with internal vibrational modes and 6 degrees of freedom for rigid body motion. Eventually, a mechanical mock-up of the final IR would be simulated and tested.

3.3 Very Fast Feedback

The time structure of the TESLA machine allows the use of beam-beam feedback to control vibrations out to the kilohertz frequency range with only a minimal loss of luminosity [6] and no provision for mechanical vibration suppression. While the 2.8 nsec bunch structure of NLC prevents an equally complete solution to the vibration problem, the use of a conceptually similar, but faster and simpler, feedback system may help reduce the requirements on any other part of the vibration suppression system.

By putting a BPM in the extraction line of one beam, as near to the IP as possible, and using simple, radiation hard electronics to drive a strip-line kicker in the incoming beam of the other charge sign, latencies as low as 10-15 nsec may be achieved. Simulations [7] of the beam-beam deflection for the parameters of NLC beams at 1 TeV have been performed which indicate that offsets of 2 to 12 sigma in y can be corrected and the net luminosity loss per bunch train crossing reduced by a factor of six. While the practical implications of locating the electronics and electrodes near the IP must be investigated, these simulation results are encouraging.

4 Crab Cavity

If the crab cavities were not present to cause the beams to collide head-on, the luminosity would be lowered by $\sim 20\%$. The most stringent tolerance induced by the cavity concerns the timing, or phase, of the arrival of the beam and the RF pulse at the cavity. The two cavities, one one each side of the IP, must have a phase difference of less than 0.05 degree of S-band. As they will be powered by a common klystron, the phase difference is not a concern. Eventually, low power and high power tests can be carried out to confirm this.

5 Mask design

There are three masks explicitly indicated in Figure 1. The conical tungsten mask $M1$ envelopes the spiralling e^+e^- pairs produced by the beam-beam interaction. The cylindrical tungsten mask $M2$ protects the tracking volume from photons that result when the pairs strike the face of $Q1$. The length of $M2$ is fairly arbitrary at this time. The cylindrical beryllium mask at $12 < r < 15$ and $55 < z < 65$cm, shadows the innermost layer of the vertex detector from very soft charged particles produced by off energy electrons that strike the extraction beam pipe and $Q1$ and spiral back along the detector's magnetic field lines.

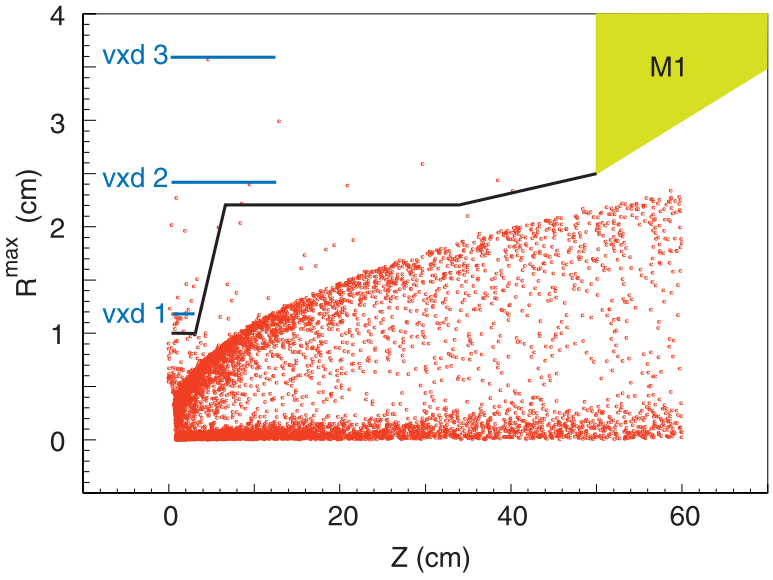

Figure 2: R^{max} vs Z distribution of pairs. Three vertex detector layers and the beam pipe are indicated.

5.1 Dead Cone

The inner angle of $M1$ is chosen so that the pairs are contained inside the tip of the mask at $z = 50$cm. A function of the detector solenoid field, the inner angle is 50 mrad for the 6 Tesla NLC small detector and 65 mrad for the 4 Tesla large detector. The outer angle of $M1$ is set at 30 mrad more than the inner angle so as to provide 6cm of transverse shielding at the face of $Q1$ at L^*=2m. The outer angle, defining what has traditionally been called the dead-cone of the IR design, is then 80 and 95 mrad for the small and large detectors, respectively. Studies have shown that 6cm is the minimal thickness to shield the inner trackers from photons produced at the $Q1$ face.

Following the lead of the TESLA collaboration, we are currently studying the implications of instrumenting the solid angle subtended by the mask $M1$ with calorimetry. The z location of the tip had been chosen to minimize rescattered SR backgrounds that enter the central tracking volume. While moving the mask tip to higher z to allow space for the calorimetery does not seem to increase detector backgrounds from the beam-beam pairs, we are studying its affect on SR backgrounds.

As Figure 2 indicates, the fact that there is a maximum p_T transvered to the pair particles because of the finite transverse size of the beam, means that there is a maximum radius for their spiraling trajectory. The luminosity monitor, which must be centered on the outgoing beam line, provides calorimetry in the angular region from the inside of $M1$ up to this maximum radius, which is about 5cm in the small detector. Hermaticity of the detector is then good up to $\cos\theta < 0.99$. Inspired by the JLC design, we plan for a pair monitor in the region between the extraction beam pipe and the luminosity monitor.

5.2 SR Masks

Figure 3 shows the photon fans from beam halo particles collimated at $8\sigma_x$ and $40\sigma_y$. For clarity, only the rays from the positive x (upper plot) or y (lower plot) orbit of the beam are drawn. Magnet apertures and masks for one incoming and extracted beam are indicated. The beamline is shown as horizontal and, in the upper plot, the detector is rotated in x by 10 mrad.

The design constraint currently being imposed on the SR masking, collimation depth, and magnet apertures is that no primary SR flux fall on either the $Q1$ aperture or the Be ring mask. By placing a 3.2mm (2.7mm) radius mask at z =12m (11m), corresponding to $8\sigma_x$ ($40\sigma_y$) beam size plus about 400 μm of clearance, the radiation from the upsream quadrupoles and soft bends is completely shielded. In x (y) some radiation from $Q2$ ($Q1$) will strike the outgoing quadruples aperture, at about 7m. The extraction line is only at a rudimentary state of engineering and background studies show that this will not be a problem for the detector. The lower plot, however, indicates that the $Q2$ produced radiation is very close to hitting the innermost tip of the $Q1$ at r = 5.9mm. Slight changes in orbit, collimation depth, or clearance could cause a problem maintaining the design goal. The plots also indicate, at z =8m (z=4m), the locations where masks could be put to shield radiation produced by the final doublet itself. This would be desireable if the $Q1$ aperture needed to be smaller or the collimation depth needed to be larger. A mask with 50 mW of power at 4m should be avoided and at present does not appear to be required.

6 Extraction Line Design Issues

The extraction line design [8] is based on the assumption that, for 1 TeV operation, a 10 MW beam dump must be placed on the neutral beam line a maximum of 150m from the IP. This distance is dictated by the maximum width of the dump window and the plan to have it accept 1 MW disrupted

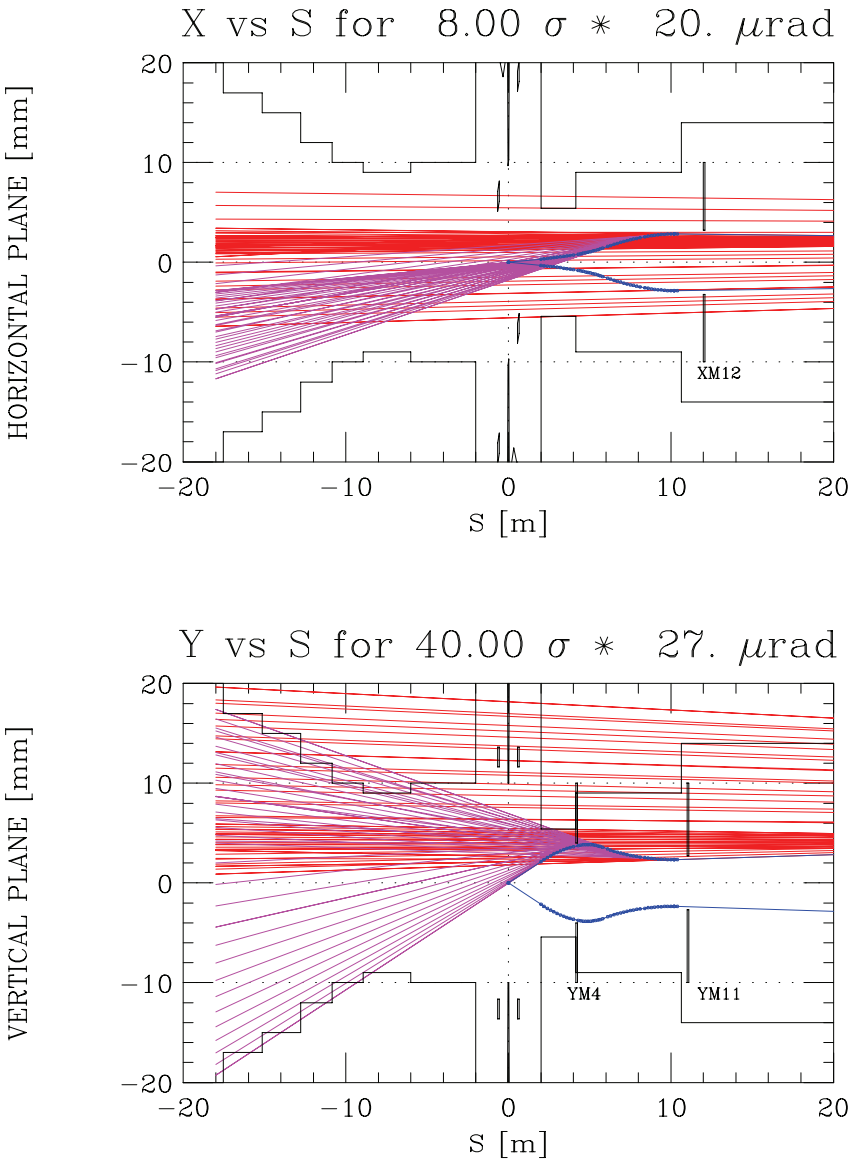

Figure 3: Photon fans from beam halo particles collimated at $8\sigma_x$ and $40\sigma_y$. For clarity, only the rays from the positive x (upper plot) or y (lower plot) orbit of the beam are drawn. Magnet apertures and masks are indicated.

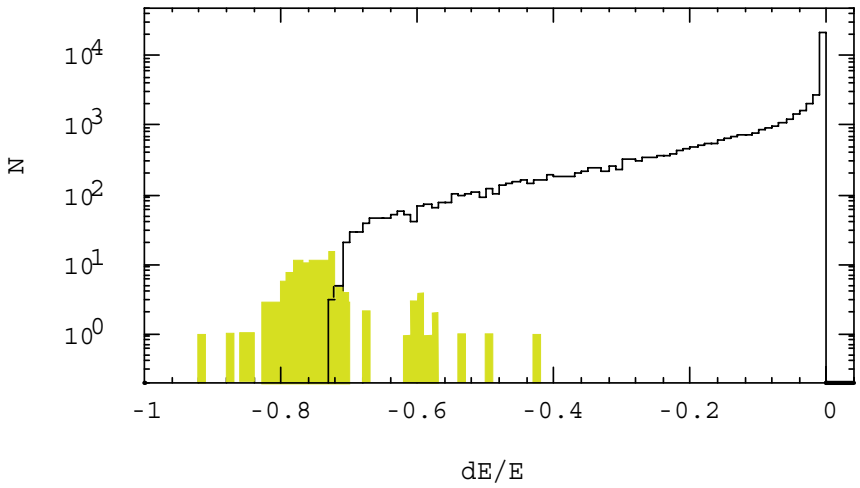

Figure 4: The energy distribution expected from the NLC 1 TeV "A" parameter set. The part of the spectrum lost in the extraction line is indicated by the shaded area.

beamstrahlung photon beam as well as the disrupted charged particle beam. The SLC experience has shown it useful to measure the beam's polarization and energy in the extraction line. To do this, a chicane has been designed which displaces the charged particle beam from the photons.

Unfortunately, the level of beam disruption forseen at the NLC is such that it is difficult to transport the entire beam cleanly to the dump. Figure 4 shows the full energy tail expected at 1 TeV for NLC parameter set "A" and that part of the tail which is lost in the line. While only amounting to 0.25% of the total number of particles, the anticipated backgrounds seem, without further study, to preclude the kinds of polarimetry and energy spectrometer used in the SLC. At 500 GeV center of mass, the disruption is less and it appears possible to use these devices. Our baseline plan is, while continuing studies, to assume that the extraction line will support beam instrumentation at the start up energy and to use beam without collisions and pre-IP diagnostics to understand the effects of the beam-beam collision. By the time the energy or luminosity has risen to the level where the beamline is in trouble, we should have understood enough to be able to trust the pre-IP instrumentation and our knowledge of the physics of the beam-beam interaction.

7 Detector Backgrounds

Detector backgrounds are calculated for the vertex detector and central tracking system in the NLC Small Detector and IR layout shown in Figure 1. Realistic three dimentional geometry together with magnetic field map for the detector solenoid and beam-line magnets are used. The complete extraction line up to the beam dump is also included in the calculation to estimate backgrounds (mostly neutrons) produced in the extraction line.

7.1 Background Sources

Detector backgrounds at the NLC are expected to come from the following sources:

Machine Backgrounds	IP Backgrounds
Direct beam loss	Disrupted primary beam*
beam-gas scattering	Beamstrahlung photons*
collimator edge scattering	e^+e^- pairs from beam-beam interactions*
Synchrotron radiation	Radiative Bhabhas*
Muons Production	Hadrons from $\gamma\gamma$ interactions
Neutron back-shine from Dump*	
Extraction Line Loss*	

Each of these sources has been described in the previous reports, and this paper describes the sources with * on which recent studies have been made. Among these sources the most dominant source is e^+e^- pairs from beam-beam interactions. The pairs are produced at the IP, interact with the beam pipe, inner vertex detector layers, mask and beamline magnets, and produce a large number of secondary e^+e^-, photons and neutrons which in turn contribute background in the vertex detector and in any tracking chamber at larger radius. In the NLC design both disrupted beam and beamstrahlung photons are extracted through a common beamline into a beam dump located at 150 m from the IP. Since the angular divergence of the beamstrahlung photons is 300 μrad, the extraction line has 1 mrad aperture so that the beamstrahlung photons do not hit the beamline aperture. In the current design, however, about 0.25% of the disrupted beam is lost in the extraction line. While the secondary e^+e^- and photons produced in the extraction line and beam dump do not contribute to the detector background, secondary neutrons are a major concern. In particular, a large number of low energy neutrons produced in the

Table 2: Background sources

Source	#particles/bunch	$< E >$ (GeV)
Disrupted Primary Beam	2×10^{10}	460
Beamstrahlung photons	3×10^{10}	30
e^+e^- pairs from Beam-Beam Interactions	8.8×10^{4}	10.5
Radiative Bhabhas	2.5×10^{5}	370

beam dump must be shielded.

7.2 Simulation Programs

Guinea-Pig is used to simulate the beam-beam interaction and to generate pairs, radiative Bhabhas, disrupted beams and beamstrahlung photons. These particles are tracked by GEANT 3 and FLUKA98 simulating electromagnetic and hadronic interactions of particles. Since GEANT 3 does not simulate photoneuclear interactions, FLUKA98 is used to calculate the neutron background. The simulations are made for 1 TeV CM machine with 1×10^{10} e^-/bunch and 95 bunches per train at 120 pps. Table 1 summarizes the number of particles per bunch and average energy.

8 Backgrounds from Beam-Beam Interaction

8.1 Pairs

Roughly 10^5 e^+e^- pairs will be produced by the beam-beam interaction each bunch crossing. The pairs with a large p_t will hit the beam pipe and vertex detector directly. But most pairs are produced with small intrinsic p_t and are curled up within 2.5 cm minimum radius of Mask M1 under the strong solenoidal magnetic field. Figure 2 shows the R^{max} vs Z distribution of pairs in 6 Tesla field where R^{max} is the first maximum radius of the helix and Z is the corresponding z-coordinate. As seen in the figure, the pair distribution has a clear boundary and the beampipe and vertex detector must be placed outside of this region. The inner most layer of the vertex detector can be placed at 1 cm, but the layer length must be short enough so that no material is inside the boundary. The beam pipe is also shaped accordingly as seen in the figure. The strong magnetic field is essential for bringing the vertex detector to a radius as small as 1 cm. There are a number of particles outside the boundary which

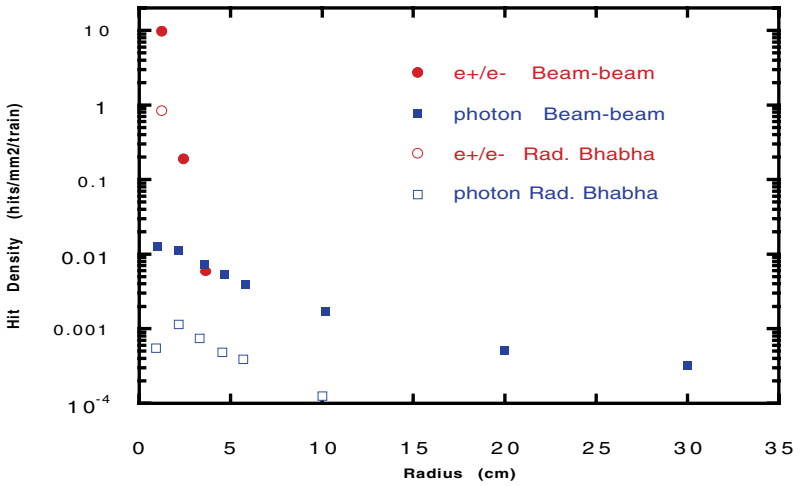

Figure 5: Charged particle hit densities as a function of radius from beam-beam pairs and radiative Bhabhas. A photon conversion efficiency of 1% is assumed.

will hit the vertex detector directly or hit the face of the M1. Although these pairs make up only 2% of produced pairs, they contribute a significant detector background as they cannot be shielded.

Figure 5 shows the hit density as a function of radius averaged over an angular acceptance of $\cos\theta = 0.92$. The hit density from radiative Bhabhas is also shown in the figure. The hit density in the inner most vertex detector layer located at r = 1.2 cm is expected to be about 10 hits/mm^2/train. Since the track linking efficiency between the vertex detector and the central tracker begins to deteriorate at the 10 hits/mm^2/train level, further reduction of the hit density is desirable. At r $>$ 2 cm, the hit density is manageable. The background contribution from radiative Bhabhas is only ten percent of the beam-beam pairs.

A recent study has revealed that the majority of the background hits in the first vertex detector layer are due to the low energy ($<$ 10 MeV) secondary particles produced in the extraction line beam pipe between $|z| = 200$ cm and 400 cm and swum back toward the IP following the solenoidal magnetic field. Since the radius of these particles is only few mm, a short (10 cm) Beryllium ring with the same radius as the vertex detector can effectively absorb them, essentially reducing the hit density to a few hits/mm^2/train level.

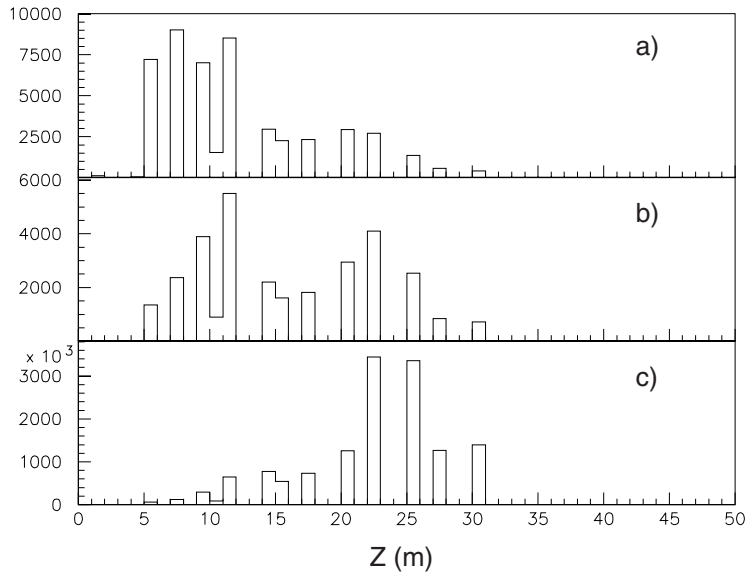

Figure 6: Neutron flux as a function of Z. a) Beam-beam pairs, b) Radiative Bhabhas, and c) Disrupted beam.

8.2 Secondary photons from Pairs

Pairs will interact with the beam pipe, inner vertex detector layers, M1 mask, and front faces of the beamline magnets. As they interact, photons will be produced which form a seconday background in the vertex detector and in any tracking chamber at larger radius. Since the energy of these photons is typically 100 keV, Si-based detectors such as CCD vertex detector and Si tracker are mostly transparent to the photons, and only converted photons contribute to detector background. Figure 5 shows the charged particle hit density of the converted photons assuming a conversion probability of 1%. The hit densities are all below $0.1/\mathrm{mm}^2$/train and have a negligible contribution to the vertex detector background. However, the hit density at r=30 cm is $3 \times 10^{-4}/\mathrm{mm}^2$/train and contributes about 0.3% occupancy for a Si Tracker with 50 μm $\times$ 20 cm multistrips. It is important to study how this background occupancy affects the tracker performance. If a low granularity tracking device such as a drift chamber were to be employed instead of Si tracker, the background occupancy is expected be too high unless more innovative masking schemes are developed.

Table 3: Neutron background in the vertex detector

Source	Hit density ($\times 10^9$ neutrons/cm^2/year)
Beam-beam pairs	1.7
Radiative Bhabhas	0.02
Disrupted beam	
Lost in ext. line	0.01
Backshine from dump	0.2
Beamstrahlung	
Backshine from dump	0.05

8.3 Secondary Neutrons

Neutrons are produced mainly through the giant-dipole resonance reaction of low energy (10 - 20 MeV) photons. The production and transport of the photoneutrons are simulated in FLUKA98. Figure 6 shows the neutron flux distribution as a function of the distance from the IP along the extraction line. The results for radiative Bhabhas and disrupted beam are also shown. Although more neutrons are produced by disrupted beams, the majority of these neutrons are produced at more than 20 m from the IP and do not contribute to the detector background. Since the beam-beam pairs produce neutrons much closer to the detector, these neutrons dominate the detector background.

When the disrupted beam and beamsrahlung photons are absorbed in the beam dump using water for the power absorption and dissipation medium, approximately 10^{24} neutrons are produced per year. While the water serves as a good neutron absorber and most of the produced neutrons are absorbed inside the dump, there are 1.5×10^{20} neutrons/year/dump coming out of the dump in the direction of the detector. Since the dump is located at 150 m from the detector, the tunnel provides a neutron attenuation of the order of 10^{-4}. The neutron background at the detector can be reduced to an acceptable level using a 2 m thick shielding wall. The neutrons coming out of the 1 mrad aperture window are potentially serious background. FLUKA98 is used to transport these neutrons and the detector background is estimated.

Table 3 summarizes the neutron background in the vertex detector. The total neutron background of 2×10^9/cm^2/year is uncomfortably close to the conservative upper limit[9] of 3×10^9/cm^2/year.

Acknowledgments

This paper contains the work of many people in the NLC Beam Delivery and Interaction Region working group, in particular, J. Frisch, J. Gronberg, S. Hertzbach, L. Keller, Y. Nosochkov, D. Schulte, K. Skarpaas, P. Tenenbaum, and M. Woods.

This work is supported in part by Department of Energy contract DE-AC03-76SF00515.

References

1. Proceedings of the 1989, 1993, and 1995 Workshops on Physics and Experiments with Linear e^+e^- Colliders, published by World Scientific.
2. The NLC Design Group, "Zeroth Order Design Report for the Next Linear Collider", *LBNL-5424, SLAC-474, UCRL-ID-124161, UC-414* (1996).
3. Proceedings of the 1996 DPF/DPB Summer Study on High Energy Physics, Snowmass '96, ed. D.G. Cassel, L. Trindle Gennari, R.H. Siemann, June 25 - July 12, 1996, Smowmass, Colorado, USA.
4. Peter Tenenbaum *et al, "New Developments in the Next Linear Collider BDS Design," SLAC-PUB-8135, Mar 1999, Contributed to IEEE Particle Accelerator Conference (PAC 99), New York, NY, 29 Mar - 2 Apr 1999.*
5. *Mike Woods, "Optical Anchor R&D for the ILC," Talk 69, LC97, Zvenigorod, Russia, Sept.29-Oct.3, 1997.*
6. *Ingrid Reyzl, this conference, "The Use of Fast Feedback at TESLA."*
7. *Daniel Schulte, LCC-0026, "Simulations of an Intra-Pulse Interaction Point Feedback for the NLC", Sept. 1999.*
8. *Y.M. Nosochkov and T.O. Raubenheimer, LCC-0034, "NLC Extraction Line Studies," 12/99.*
9. *C.J.S. Damerell and D.J. Jackson, "Vertex Detector Technology and Jet Flavour Identification at the Future e^+e^- Linear Collider." in Ref. 1.*